

# Tailor-made magnetic nanocarriers with pH-induced charge reversal and pH-responsiveness to guide subcellular release of doxorubicin

Han Zhang · Yanan Xue · Juan Huang · Xiaoyang Xia · Meifang Song · Kaikai Wen · Xiaoxiao Zhang · Xiaogang Luo · Ning Cai · Sihui Long · Faquan Yu

Received: 7 September 2014 / Accepted: 15 December 2014 / Published online: 30 December 2014  
© Springer Science+Business Media New York 2014

**Abstract** A charge reversible, magnetic-targeted, and pH-responsive nano therapy system assembled from citraconic-modified dextran (Dex–COOH), glycine-stabilized superparamagnetic iron oxide nanoparticles (SPION–NH<sub>2</sub>), and doxorubicin (DOX) through electrostatic interaction was designed for delivering therapeutics to tumor cells. Dex–COOH was first synthesized to build the pH-sensitive citraconic amide bond and further render charge reversal upon the cleavage of the linkage. The SPION–NH<sub>2</sub> anchored in the nanocarrier endows the carrier with magnetic migration. The vibrating sample magnetometer analysis exhibits the superparamagnetic behavior, and the magnetic saturation value is estimated to be 39.6 emu (g Fe)<sup>-1</sup>. The change of size and the reversal of zeta potential from negative to positive in acidic environment confirmed these expected responsibilities. The DOX-loaded nanocarriers contain DOX up to 13.0 wt%. An in vitro release profile demonstrated an efficient DOX release of 80 % at pH 5.0 while of 27 % at pH 6.8 and 13 % at pH 7.4, suggesting a pH-induced release mechanism. Microscopic images of Prussian blue staining, quantification of cellular iron and protein concentration displayed apparent iron uptake by HeLa cells. Confocal laser scanning

microscopy observations revealed that the nanocarriers could efficiently deliver and release DOX into the nuclei of HeLa cells. MTT assays testified that DOX-loaded nanocarrier exhibited high anti-tumor activity with IC<sub>50</sub> of 0.7 μg mL<sup>-1</sup>, while plain nanocarriers were practically non-toxic. This drug delivery system has shown the ability to improve the chemotherapeutic efficacy and to reduce the side effects, indicating great potential for delivery of drugs to the targeted sites in patients.

## Introduction

Recently, many efforts have been made for efficient delivery of therapeutics into tumor cells to increase the intracellular drug concentration at targeted site. Stimuli-responsive delivery systems have received intensive attention because they offer a promising approach to maximize therapeutic activity while minimizing adversary effects [1]. Of these stimuli, pH-responsiveness is one of the mostly applied strategies for achieving this purpose [2]. It is well known that the environments of cancerous tissues (pH 6.5–7.2), endosomes (pH 5.0–6.5), and lysosomes (pH 4.5–5.0) are more acidic than those of blood and normal tissues (pH 7.4) [3–5]. Once being endocytosed, the drug carriers will experience a pH drop from 7.4 to around 6.0 in the early endosomes. By utilizing the variations above, drug delivery systems have the potential to trigger drug release responding to the pH values in the body. Jousheed and co-workers reported the use of red-emitting conjugated oligomer-based pH-responsive nanoparticles could provide a sustained drug release in the physiological pH but enable fast release at low pH, a micro environment found in tumor [6]. Shi et al. reported using a doxorubicin (DOX)-loaded poly(ethyleneimine) (PEI)-derived fullerene (C<sub>60</sub>-PEI-

H. Zhang · Y. Xue · J. Huang · X. Xia · M. Song · K. Wen · X. Luo · N. Cai · S. Long · F. Yu (✉)

Key Laboratory for Green Chemical Process of Ministry of Education, Hubei Provincial Key Lab of Novel Reactor and Green Chemical Technology, School of Chemical Engineering and Pharmacy, Wuhan Institute of Technology, Xiongchu Ave 693, Wuhan 430073, Hubei, China  
e-mail: fyuwucn@gmail.com; fyu@mail.wit.edu.cn

X. Zhang  
Department of Chemical and Biological Engineering, Zhejiang University, Hangzhou 310027, China

DOX) to facilitate chemotherapy, in which DOX was covalently conjugated onto C<sub>60</sub>-PEI by the pH-sensitive hydrazone linkage. The release profiles of DOX from C<sub>60</sub>-PEI-DOX showed a strong dependence on the environmental pH value [7]. These studies have demonstrated the pH-responsive nanoparticles could be used for tumor-targeting DOX delivery [8].

Positively charged nanocarriers show higher affinity toward negatively charged plasma membranes, and are estimated to be more readily internalized than negatively charged nanocarriers [9]. Nonetheless, the former intensely interacts with serum components in the bloodstream, thus is not suitable for *in vivo* application on account of its enhanced non-specific cellular uptake, which probably leads to serious aggregation and rapid clearance from circulation [10, 11]. In contrast, negatively charged nanocarriers have shown long circulation by virtue of potential protein resistance. Consequently, to create negatively charged nanocarriers in the process of blood circulation and to convert them into positively charged ones in tumor would make great sense. A hopeful way is to utilize the acidic tumoral extracellular environment as a trigger to reverse the nanocarrier from negative to positive surface charge upon the arrival of drug carriers at target sites [12–15]. The advantages of realizing the charge reversal in light of *in situ* acidic environment are obvious. Zhou recently reported this kind of nanocarriers in which negative charge decreased with the change of pH from 7.4 to 6.8 and finally became positive at pH 5.0 [16]. The nanocarriers were negatively charged to avoid the clearance from circulation and later converted into positive charge for high cellular uptake.

In addition, magnetic nanoparticles have been studied for their potential applications in a wide range of biomedical fields, such as magnetic resonance imaging (MRI) and targeted drug delivery [17]. The uptake of the magnetic nanoparticles can be enhanced by guiding the nanoparticles to the cells with the aid of a pulsed magnetic field [18–20]. The incorporation of superparamagnetic feature into pH-responsive nanocarrier is a promising strategy for the purpose of targeting by virtue of an external magnetic field to direct the magnetic nanoparticle to the regions of interest.

In this study, superparamagnetic iron oxide nanoparticles (SPION) were first prepared by a co-precipitation method. Dextran was modified by the incorporation of a citraconic lateral chain via a three-step process. The citraconic lateral chain is known to be sensitive to mild acid and can be cleaved readily in that environment [21]. This chain is widely applied as a convenient linkage to fabricate a device with acid sensitivity. Interestingly, the linkage will recover positive amino groups upon the cleavage of amide bond, resulting in charge reversal [22]. The designed

nanocarrier, comprising magnetic SPION and pH-sensitive dextran derivatives (Dex-COOH), endows pH-responsiveness, superparamagnetic behavior, and pH-triggered charge reversal (Scheme 1). The *in vitro* release was evaluated under a wide variety of conditions, and the cell viability and the behavior of cellular uptake were assayed in terms of cell study.

## Experimental sections

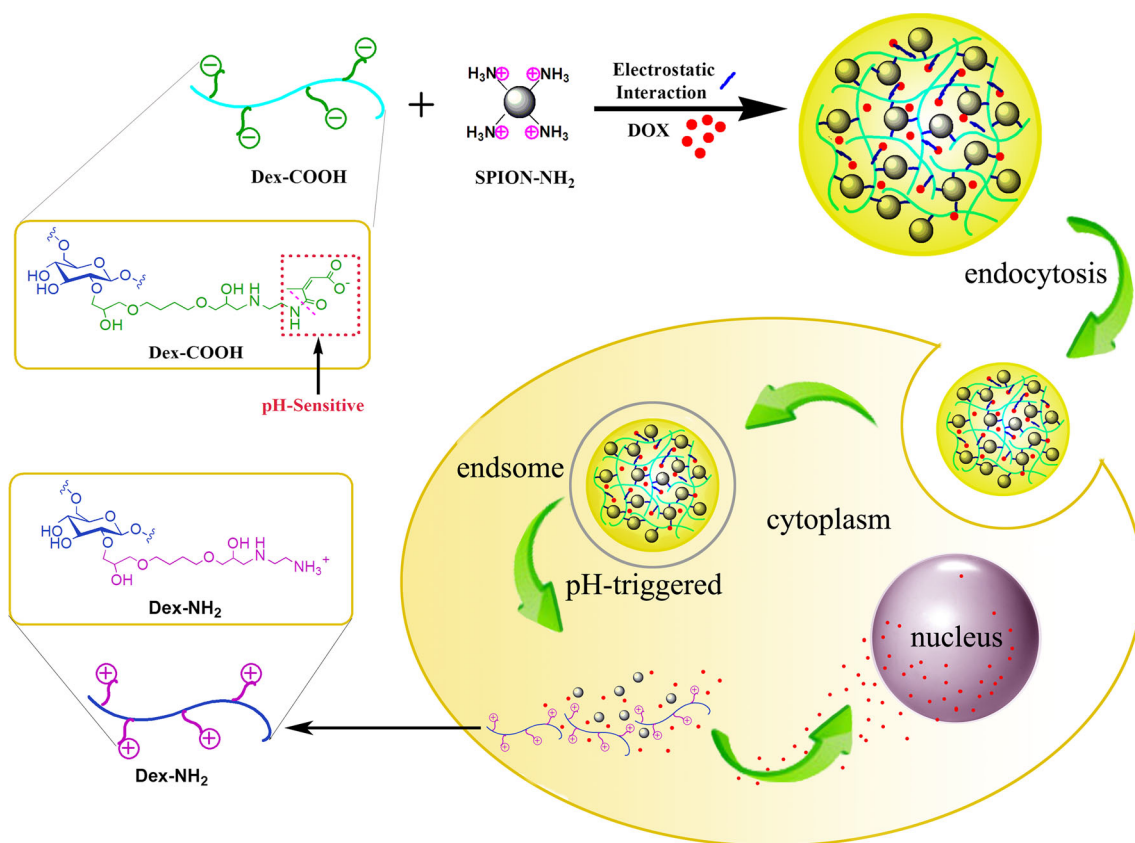
### Materials and cell lines

Dextran (70 kDa), 1,4-butanediol diglycidyl ether (95 %), ethylenediamine dihydrochloride (EDA·2HCl, 98 %), citraconic anhydride (98 %), sodium borohydride (NaBH<sub>4</sub>, 98 %), and glycine (98.5 %) were purchased from Aladdin Industrial Co. Iron (II) chloride tetrahydrate (FeCl<sub>2</sub>·4H<sub>2</sub>O, 98 %), iron (III) chloride hexahydrate (FeCl<sub>3</sub>·6H<sub>2</sub>O, 97 %), picrylsulfonic acid solution (TNBS, 5 % (w/v) in ddH<sub>2</sub>O), potassium hexacyanoferrate (II) trihydrate (98.5 %), potassium thiocyanate (KSCN, 99 %), paraformaldehyde (95 %), hoechst 33258, and 3-[4,5-dimethylthiazol-2-yl]-2,5-diphenyltetrazolium bromide (MTT) were purchased from Sigma-Aldrich. Tetrahydrofuran (THF), dimethyl sulfoxide (DMSO), and dialysis tubing (MWCO 8000–14000) were purchased from Sinopharm Chemical Reagent. Doxorubicin hydrochloride (DOX·HCl, >98 %) was purchased from Arking Pharma Scientific. All chemicals were used as received without further purification. Ultrapure water was prepared by Heal Force super NW water purification system (Heal Force Development Ltd.).

HeLa cells were purchased from the China Center for Type Culture Collection (Wuhan University) and cultured in RPMI-1640 (Gibco) supplemented with 10 % fetal bovine serum (FBS, Hyclone) and 1 % antibiotics (100 U mL<sup>-1</sup> penicillin and 100 µg mL<sup>-1</sup> streptomycin) at 37 °C in a humidified atmosphere containing 5 % CO<sub>2</sub>.

### Instruments

Fourier transform infrared (FTIR) spectra were recorded on a Nicolet 5700 spectrometer in the wavenumber range of 400–4000 cm<sup>-1</sup>. Samples were ground with KBr and pressed to plates for measurement. <sup>1</sup>H nuclear magnetic resonance (<sup>1</sup>H NMR) spectra were recorded on a Bruker Avance-500 spectrometer using D<sub>2</sub>O as solvent. The size, size distribution, and zeta potential were investigated by dynamic light scattering (DLS) using a Zetasizer ZEN3690 (Malvern) with a He–Ne laser beam at 633 nm at 25 °C. Morphology of nanocarrier was observed under a transmission electron microscope (TEM) using Tecnai G2S-



**Scheme 1** Illustration of formation, endocytosis and pH-triggered dissociation of DOX-loaded pH-MN

Twin at an accelerating voltage of 200 kV. Around 5  $\mu\text{L}$  of the nanocarrier suspension was placed on a copper grid. The grid was allowed to dry at room temperature overnight. The magnetic property of DOX-loaded nanocarrier was evaluated on a vibrating sample magnetometer (VSM, Westerville, OH, USA) via changing the magnetic field from  $-20000$  to  $20000$  Oe at  $25^\circ\text{C}$ .

#### Synthesis of glycine-modified superparamagnetic iron oxide nanoparticles (SPION-NH<sub>2</sub>)

SPION-NH<sub>2</sub> was synthesized following a previous publication with a minor modification [23]. In brief, glycine (7.5 g, 0.1 mol) was dissolved in 500 mL NaOH ( $3\text{ mol L}^{-1}$ ), which was purged under a flow of nitrogen for 0.5 h. An ionic solution (45 mL) containing  $0.76\text{ mol L}^{-1}$  of FeCl<sub>3</sub> and  $0.4\text{ mol L}^{-1}$  of FeCl<sub>2</sub> (molar ratio of ferric to ferrous was approximately 2:1) was prepared in HCl at pH 1.7 under nitrogen protection. The ionic solution was then added dropwise to the glycine alkaline solution mentioned above under vigorous mechanical stirring. This reaction mixture was gradually heated ( $1^\circ\text{C min}^{-1}$ ) to  $78^\circ\text{C}$  and held at this temperature for 1 h under stirring and nitrogen protection. After

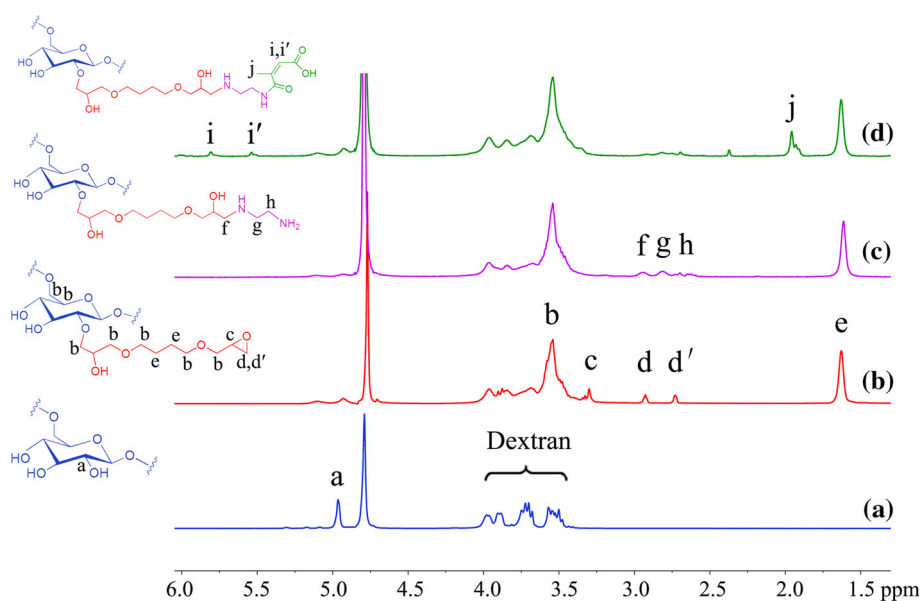
separation of the supernatant with a permanent magnet, the wet solid collection was further purified by washing with ultrapure water multiple times till the unreacted glycine was removed completely. Finally, the product was redispersed with pH 3.0 HCl and the concentration of SPION-NH<sub>2</sub> solution was adjusted to  $1\text{ mg Fe mL}^{-1}$ .

#### Synthesis of negatively charged dextran with acid cleavable side chain (Dex-COOH)

Synthesis of dextran with a side chain of an acid cleavable citraconic amide group was conducted by a three-step process (Fig. 1).

First, the epoxy-activated dextran (Dex-EPO) was synthesized by a ring-opening reaction of 1,4-butanediol diglycidyl ether initiated by the hydroxyl groups of dextran. Briefly, dextran (0.348 g, 2.0 mmol in terms of glucosyl units) was dissolved in a 10 mL mixture of NaOH ( $0.6\text{ mol L}^{-1}$ ) and NaBH<sub>4</sub> ( $2.0\text{ mg mL}^{-1}$ ). The dextran solution was then added dropwise to 60 mL 1,4-butanediol diglycidyl ether solution ( $1.7\text{ mol L}^{-1}$ ) under vigorously stirring and the reaction was kept at  $37^\circ\text{C}$  for 12 h. After that, the resultant solution was dialyzed against ultrapure water for 3 days and lyophilized. The amount of epoxy

**Fig. 1**  $^1\text{H}$  NMR spectra of dextran (a), Dex-EPO (b), Dex-NH<sub>2</sub> (c), and Dex-COOH (d), using D<sub>2</sub>O as solvent



groups incorporated on dextran was determined by Axen method [24].

Subsequently, the amino-modified dextran (Dex-NH<sub>2</sub>) was obtained through a ring-opening reaction of the terminal epoxy group of Dex-EPO initiated by the amino group of EDA·2HCl. In brief, Dex-EPO (2.0 mmol in terms of glucosyl units) reacted with excess amount of EDA·2HCl (20 mmol) in pH 10 carbonate-bicarbonate buffer (0.2 mol L<sup>-1</sup>) under vigorous stirring at 25 °C for 48 h. Then, the resultant solution was dialyzed against ultrapure water for 3 days and lyophilized. The reaction conversion was determined both by the TNBS method [25] for amine groups and the Axen method for epoxy groups remained [24].

Finally, to obtain the dextran with acid cleavable side chain (Dex-COOH), Dex-NH<sub>2</sub> was further conjugated with citraconic anhydride to introduce pH-sensitive citraconic amide groups. In short, 50 mL citraconic anhydride (7 mg mL<sup>-1</sup>) in THF was added dropwise to 72 mL Dex-NH<sub>2</sub> (4.8 mg mL<sup>-1</sup>) in phosphate-buffered saline (PBS, 0.2 mol L<sup>-1</sup>) at pH 8 under vigorous stirring for 10 h at 25 °C. Then, the mixture was dialyzed against PBS buffer (0.1 mol L<sup>-1</sup>) at pH 8 at room temperature for 3 days and dialyzed against pH 7.4 NaOH solution for 12 h. After purification, the product Dex-COOH was lyophilized. The degree of substitution (DS) of Dex-COOH reflected as the molar ratio of carboxyl groups incorporated into the glucosyl units of dextran was calculated by measuring the carboxyl groups using acid–base titration method [26].

#### Preparation of pH-sensitive magnetic nanocarriers

The self-assembled pH-sensitive magnetic nanocarriers were prepared through the electrostatic interaction between

pendent carboxyl groups in Dex-COOH and amino groups on the surface of SPION-NH<sub>2</sub>.

In a typical procedure, DOX·HCl (6 mg) was mixed with 10 mL SPION-NH<sub>2</sub> suspension (1 mg Fe mL<sup>-1</sup>). After being adjusted to pH 5.0 with 1 mmol L<sup>-1</sup> HCl, the suspension was added dropwise to the Dex-COOH solution (2 mg mL<sup>-1</sup> in NaOH, pH 10). The mixture solution was maintained at pH 7.4 by adjusting with 0.1 mol L<sup>-1</sup> NaOH and stirred for 6 h. Finally, the solution was transferred to dialysis tubing and purified by dialysis against ultrapure water. The entire procedure was performed in the dark at room temperature. The DOX-loaded nanocarriers, named as DOX-loaded pH-MN, was stored at 4 °C and used directly for other tests. In experiments, the weight ratio of Dex-COOH over SPION-NH<sub>2</sub> was regulated in 2/1, 1/1, and 1/2, corresponding to the sample code with DOX-loaded pH-MN2/1, DOX-loaded pH-MN1/1, and DOX-loaded pH-MN1/2 (as Table 1), respectively, with the amount of DOX and the sum amount of Dex-COOH and SPION-NH<sub>2</sub> fixed. Plain nanocarriers, named as pH-MN, without DOX included in the preparation process, was produced in the same way.

To determine the drug-loading content (DLC) and drug loading efficiency (DLE), the DOX-loaded nanocarriers were freeze-dried and quantified. The amount of DOX loaded in nanocarriers was determined by referring to the fluorescent characteristic of DOX (excitation at 480 nm and emission at 590 nm) using a calibration curve constructed from DOX solutions. The equations were as follows:

$$\text{Drug loading content (\%)} = \frac{W_{\text{drug}}}{W_{\text{nanocarrier}}} \times 100 \%$$

$$\text{Drug loading efficiency (\%)} = \frac{W_{\text{drug}}}{W_{\text{fed drug}}} \times 100 \%$$

**Table 1** Composition and characteristics of pH-MNs

Sample code	Fed ratio			Nanoparticle				
	Dex-COOH (mg/mL)	SPION-NH <sub>2</sub> (mg/mL)	DOX·HCl (mg/mL)	Size (nm)	PdI	Zeta potential (mV)	DLC (%)	DLE (%)
pH-MN	0.8	0.4	–	112.5±15.0	0.155	–24.3±2.5	–	–
DOX-loaded pH-MN2/1	0.8	0.4	0.24	138.5±2.1	0.133	–22.3±1.7	13.0	74.9
DOX-loaded pH-MN1/1	0.6	0.6	0.24	137.6±13.3	0.234	–24.5±2.2	11.9	67.4
DOX-loaded pH-MN1/2	0.4	0.8	0.24	102.1±9.3	0.204	–24.3±0.6	9.4	52.1

All of the nanocarriers were prepared under pH 7.4 with 6 h stirring. DLC and DLE are abbr. for drug loading content and efficiency, respectively

where  $W_{\text{nanocarrier}}$  was the weight of lyophilized nanocarriers after dialysis,  $W_{\text{drug}}$  was the weight of DOX loaded in the nanocarriers, which was taken as the total released weight of DOX from nanocarriers, and  $W_{\text{fed drug}}$  was the fed weight of DOX·HCl.

#### In vitro DOX release

The release behavior of DOX-loaded nanocarriers under different pH conditions was evaluated using the following procedure. Freeze-dried samples (20 mg) were suspended in 5 mL PBS (0.1 mol L<sup>-1</sup>) at pH 7.4, and transferred to a dialysis tubing, which was immersed into 15 mL PBS (0.1 mol L<sup>-1</sup>) at pH 5.0, 6.8, or 7.4, respectively. The release experiment was conducted in a water bath with a shaking rate at 60 rpm at 37 °C. At predetermined intervals, 2 mL of the incubated solution was taken out and replaced with 2 mL of corresponding fresh buffer solution. The amount of DOX released was evaluated by fluorescence spectrometer as mentioned in “Preparation of pH-sensitive magnetic nanocarriers” section. All measurements were performed in triplicate.

#### Cytotoxicity evaluation

MTT assay was used to evaluate the cytotoxicity of the nanocarriers. HeLa cells were seeded into 96-well plates at a density of ~5000 cells per well in 100 µL complete RPMI-1640 containing 10 % FBS and cultured for 1 day at 37 °C in 5 % CO<sub>2</sub> atmosphere. Then, 100 µL solution of pH-MN or DOX-loaded pH-MN nanocarriers, that were serially diluted in complete RPMI-1640 in different concentrations ranging from 3×10<sup>-3</sup> µg mL<sup>-1</sup> through 60 µg mL<sup>-1</sup>, was separately loaded into each well. Meanwhile, the control wells were loaded with fresh complete RPMI-1640 without nanocarriers. After 48 h incubation, the culture medium was disposed, and the cells were washed with PBS (0.01 mol L<sup>-1</sup>) at pH 7.4. Subsequently, 100 µL culture medium and 20 µL MTT solution

(5 mg mL<sup>-1</sup> in PBS) were added to each well. In above procedure, blank wells were designed by substituting PBS solution for MTT solution. After further incubation for 4 h, the medium was removed and 150 µL of DMSO was added to dissolve the formazan blue crystal. The absorbance of the solution in each well at 570 nm was measured using a microplate reader (Bio-Rad 550, Hercules). The percentage relative cell viability in reference to control wells containing complete RPMI-1640 without nanocarriers was calculated by the following equation:

$$\text{Relative cell viability (\%)} = \frac{A_{\text{sample}} - A_{\text{blank}}}{A_{\text{control}} - A_{\text{blank}}} \times 100 \%$$

Relative cell viability graphs were plotted against the concentration of nanocarriers. Data were presented as average ±SD ( $n = 8$ ).

#### Cellular uptake of the nanocarriers

##### Quantitative cellular uptake of iron

The quantification of intracellular iron concentration was determined by a colorimetric method depending on the formation of red-colored iron compound produced by the complexation reaction between iron and thiocyanate ion [27]. HeLa cells were seeded into 6-well plates at a density of ~2×10<sup>5</sup> cells per well and cultured for 1 day to adhere to the well bottom. Subsequently, the culture medium was replaced with 4 mL of fresh medium containing DOX-loaded pH-MN2/1 nanocarriers of different concentrations. Wells only containing cell culture medium were prepared as control. After incubation for 24 h, the cells were washed with PBS, trypsinized, and finally dispersed in 1 mL of ultrapure water. The cell suspension was divided into two aliquots. One aliquot was used for measurement of iron concentration. After the cell suspension was centrifuged at 1500 rpm for 3 min, the collected cell pellets were dissolved in 37 % HCl solution and diluted to give a final 12 % HCl solution. The HCl-treated solution was then



centrifuged at 12000 rpm for 10 min to collect clear supernatant. Finally, 100  $\mu\text{L}$  of the supernatant was added into a 96-well plate, and 100  $\mu\text{L}$  of 0.1 mol  $\text{L}^{-1}$  KSCN solution was added into the wells and incubated for 5 min to form the red iron-thiocyanate. The absorption was read by a microplate reader at a wavelength of 490 nm. The quantification of iron concentration was calculated according to a calibration curve acquired from iron chloride solution. The value of intracellular iron content was normalized against the protein amount of corresponding cells. The protein amount was quantified with the other aliquot of the test sample, which was determined by a BCA assay kit (Promega). All measurements were performed in triplicate.

#### *Prussian blue staining*

Prussian blue staining was used as a qualitative and visual method to observe the intracellular iron distribution. HeLa cells were seeded into 24-well plates at a density of  $\sim 5 \times 10^4$  cells per well in 1 mL complete RPMI-1640 containing 10 % FBS and cultured for 1 day at 37 °C in 5 %  $\text{CO}_2$  atmosphere. Then, the culture medium was replaced with 1 mL of fresh medium containing 1.2  $\mu\text{g}$  of nanocarriers. For control cells, no nanocarriers were applied. After 24 h incubation, the cells were washed thrice with PBS (0.01 mol  $\text{L}^{-1}$ , pH 7.4) and fixed for 10 min using 4 % (w/v) paraformaldehyde at room temperature. After washing thrice with PBS, the cells were stained with 1 mL of freshly prepared 4 % potassium ferrocyanide and 8 % HCl solution for 30 min at 37 °C. Finally, the stained cells were washed thrice with PBS and visualized by a reverse microscope (Ti, Nikon, Japan).

#### *Confocal laser scanning microscopy (CLSM) observation*

CLSM was employed to visualize the intracellular distribution of DOX. HeLa cells were seeded in the culture dish with a coverslip at a density of  $\sim 2 \times 10^5$  cells per well and cultured for 1 day. The cells were then incubated with DOX-loaded pH-MN2/1 nanocarriers for 4 h or 24 h at 37 °C. The final concentration of DOX-loaded pH-MN2/1 nanocarriers and DOX from the nanocarriers was 5.4 and 0.7  $\mu\text{g mL}^{-1}$ , respectively. At predetermined time, the culture media were subsequently removed, and the cells were washed thrice with PBS and fixed with 4 % (w/v) paraformaldehyde for 10 min at room temperature. The slides were then rinsed thrice with PBS. Finally, the cells were stained with Hoechst 33258 (5 mg  $\text{mL}^{-1}$  in PBS) at 37 °C for 10 min. After further rinsing with PBS thrice, the prepared slides were examined by CLSM (Nikon, TE2000, EZ-C1, Japan).

## Results and discussion

### Preparation and characterization of DOX-loaded pH-MN

The process of formation and dissociation of the designed DOX-loaded nanocarriers is represented in Scheme 1. SPION- $\text{NH}_2$  and Dex-COOH were, respectively, synthesized to achieve a pair of oppositely charged precursors. SPION- $\text{NH}_2$ , Dex-COOH, and DOX·HCl were then loaded together for the preparation of pH-MN by electrostatic attraction between the amine group and the carboxylic group. The negative charge-carrying carboxyl groups in Dex-COOH tend to bind the positive charge-carrying amino groups provided by both SPION- $\text{NH}_2$  and DOX, resulting in the self-assembly of nanocarriers and in the enhanced drug-loading capacity.

The electrostatic interaction will be destroyed, in one respect, and citraconic anhydride side chain pending on dextran will be cleaved [21], in another respect, when the nanocarriers are transferred to a mildly acidic department, like endosome or tumor. Both of these caused the disassembly of the DOX-loaded pH-MN and triggered the release of DOX correspondingly. More importantly, pH-MN undertook surface charge reversal during the process of disassembly, presumably due to the cleavage of citraconic amide in Dex-COOH under acidic pH. The cleavage produced amino groups after the elimination of carboxylic group from citraconic amide [22] (see Scheme 1). The charge reversal was in turn beneficial to enhancing the uptake efficiency of DOX.

### *Synthesis and characterization of SPION- $\text{NH}_2$*

SPION- $\text{NH}_2$  was synthesized following a reported procedure [23]. The treatment of the bare SPION, produced previously [28], with glycine yielded SPION- $\text{NH}_2$ . This process is based on the formation of a covalent bond of Fe-O-C [29]. Glycine was used here to create surface positive charge on SPION since a free amine group remained once glycine was conjugated via the Fe-O-C bond [30]. The average hydrodynamic size of SPION- $\text{NH}_2$  was determined to be  $21.6 \pm 1.7$  nm by the DLS method, with zeta potentials of  $+28.3 \pm 2.4$  mV in pH 3.0 HCl medium.

### *Synthesis and characterization of Dex-COOH*

The synthetic scheme of citraconic anhydride-modified dextran (Dex-COOH) is shown in Fig. 1. Three steps were adopted. First, the monomer of 1,4-butanediol diglycidyl ether was used to incorporate active epoxy groups into dextran side chain in alkali condition through the ring-opening reaction of epoxy groups by the hydroxyl groups

on dextran (Dex–EPO). A 50-fold excess amount of the monomer was applied with an attempt to avoid cross-linking and to ensure the free terminal epoxy groups on lateral graft chain. Then, the epoxy groups reacted with ethylenediamine at pH 10 to obtain amino-terminated dextran (Dex–NH<sub>2</sub>). Finally, citraconic anhydride was attached to dextran via the ring-opening reaction of anhydride with the amino groups of Dex–NH<sub>2</sub>, forming the pH-cleavable citraconic amide (Dex–COOH).

The successful synthesis of the dextran derivatives was confirmed by <sup>1</sup>H NMR and FTIR measurements. The <sup>1</sup>H NMR spectra of dextran, Dex–EPO, Dex–NH<sub>2</sub>, and Dex–COOH are shown in Fig. 1. Consistent with the results in references [31], unmodified dextran expressed typical signals between 3.30 and 3.98 ppm and at 4.96 ppm (peak a in Fig. 1a). In Fig. 1b, peak c (3.32 ppm) was attributed to the methylene protons, and both peak d (2.95 ppm) and peak d' (2.75 ppm) were attributed to the methine protons in epoxy groups. Further, peak b (3.56 ppm) and peak e (1.64 ppm) were assigned to the signal of methylene protons in the side chain. Therefore, the existence of terminal epoxy group was confirmed. In Fig. 1c, the signals belonging to epoxy groups (peaks c, d, and d') disappeared but three new peaks appeared between 2.61 and 2.94 ppm (peaks f, g, and h). These new peaks were assigned to the protons of the ethylenediamine chain. The observation confirmed the success of reaction. The integral ratios of peak f to peak g or peak h were estimated to be 1:0.97 or 1:0.96, close to 1:1. This demonstrated the peak assignment is reliable. The final product, Dex–COOH, was analyzed and confirmed as follows (in Fig. 1d):  $\delta$  (ppm) = 1.93 (peak j, 3 H, s, COCHCCH<sub>3</sub>COOH), 5.6 (peak i', proximal isomer, 0.46 H, s, COCCH<sub>3</sub>CHCOOH), and 5.8 (peak i, distalisomer, 0.54 H, s, COCHCCH<sub>3</sub>COOH). These are in good accordance with a previous report [32].

Figure 2 shows the FTIR spectra of the aforementioned dextran derivatives. The absorbance at 1655 cm<sup>-1</sup> is due to the hydrogen bonding in dextran [33]. The exhibition of the characteristic peak corresponding to the epoxy ring at 1250 cm<sup>-1</sup> suggested the successful synthesis of Dex–EPO. The disappearance of the characteristic peak of epoxy ring and the appearance of the vibration peak of amine groups appeared at ~1500 cm<sup>-1</sup> [34] in the synthesis of Dex–NH<sub>2</sub> evidenced the expected Dex–NH<sub>2</sub>. The existence of peak at 1700 cm<sup>-1</sup> due to the C=O stretching vibration of the carboxylic groups and the peak at 1650 cm<sup>-1</sup> assigned to C=O group of citraconic amide, which was absent in Dex–NH<sub>2</sub>, also confirmed the preparation of Dex–COOH.

The DS is defined as the number of functional groups introduced in each glucosyl unit of dextran. Axen's acid–base titration method was used to determine the amount of epoxy groups in Dex–EPO [24]. The DS of epoxy group

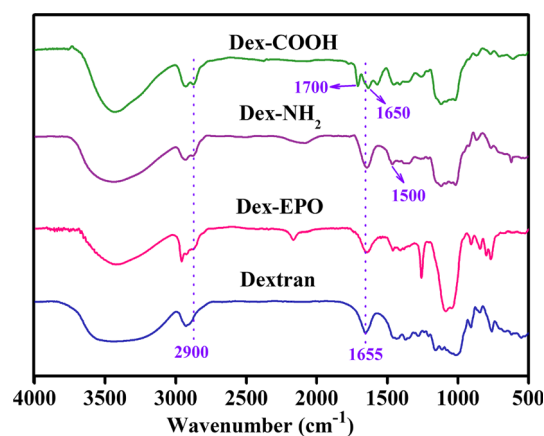


Fig. 2 FTIR spectra of the dextran derivatives

was approximately 0.33. TNBS method was used to determine the amount of amino groups [25], and the DS of amino group was estimated to be 0.28. Further, the carboxyl groups were quantitatively titrated [26], and the DS was found out to be 0.25.

#### Formation of DOX-loaded pH-MN

In the formation of nanocarriers, a group of formulations were investigated with an attempt to demonstrate the flexibility of the preparation technique (Table 1).

The size of nanoparticles is a crucial parameter for intracellular drug delivery, because small-sized nanoparticles (<200 nm) are beneficial to the maintenance of low-level reticuloendothelial system uptake, minimal renal excretion, and facile-enhanced permeability and retention (EPR) effect for passive tumor targeting [35, 36]. In order to obtain a nanocarrier with a suitable size, a set of preparation parameters were tested, including pH, stirring time, concentration, and feeding ratio. To avoid the cleavage of citraconic amide in Dex–COOH during preparation procedure, pH 7.4 was chosen as the optimal condition for pH-MN formation. The optimized conditions are shown in Table 1.

The obtained size is in the range of 100–140 nm under the preparation conditions. The DLS measurement displayed a single-peak size distribution (Fig. 3a). This is the ideal size range for the application as a drug carrier. This testified that the nanocarriers can be easily controlled in size in terms of synthesis conditions. TEM images (Fig. 3b) illustrated the size and morphology. The DLS size is in accordance with the observation in TEM images. The uneven morphology is obvious and was usually observed, consistent with many other works [37–39]. The abundant negative surface charges stabilize the particle efficiently though the particle is uneven. The nanocarrier contains many small and dark particles (inset in Fig. 3b).

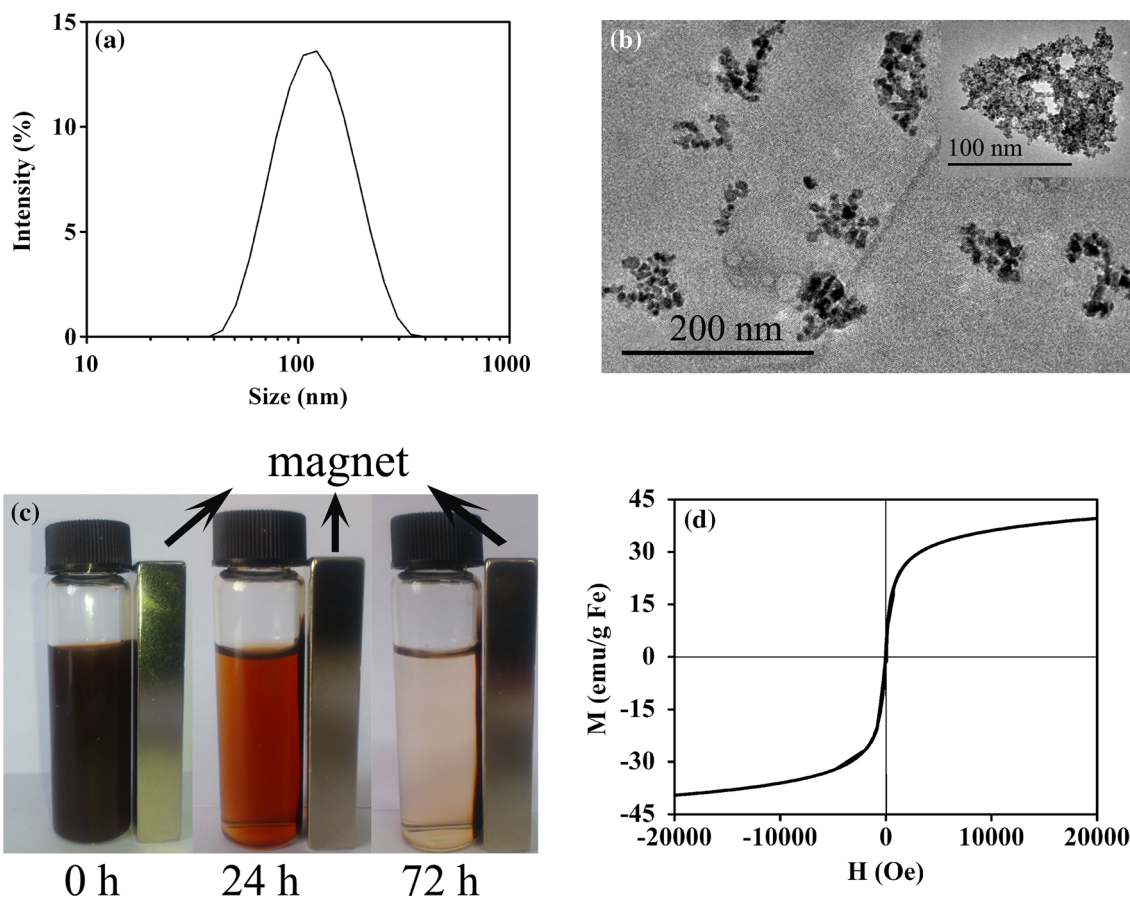


**Fig. 3** Characterization of DOX-loaded pH-MN2/1: hydrodynamic size distribution (a), TEM micrographs (b), magnetophoresis photograph exposed to a magnet for 0, 24, and 72 h (c) and VSM spectrum (d)

The latter was believed to be SPION which were densely packed together. This is regarded as the source of superparamagnetism.

The zeta potential was revealed to be around  $-22 \sim -25$  mV (Table 1). For instance, the DOX-loaded pH-MN2/1 exhibited a negative charge of  $-22.3$  mV. These data demonstrate that sufficient carboxyl groups exist on the surface of nanocarriers, which in turn guard against the aggregation and stabilize the nanocarriers in storage through the electrostatic repulsion forces between the negative charges.

Due to the incorporation of SPION, the pH-MN nanocarrier was anticipated to show magnetophoresis under an external magnetic field. Figure 3c displays the visual variation in color after being exposed to a magnet. It was observed that dark matter was gradually enriched at the site of the magnet with the prolongation of exposure time. The suspension fluid changed light in color from dark (0 h) to brown (24 h) to almost colorless (72 h). The VSM results, shown in Fig. 3d, demonstrated that the nanocarrier exhibited superparamagnetic properties, without remnant hysteresis loop in the magnetization/demagnetization curves. The saturation

magnetism for the DOX-loaded pH-MN2/1 was estimated to be  $39.6 \text{ emu (g Fe)}^{-1}$ . This is a significant property for a magnetic nanocarrier. When the external magnetic field was removed, superparamagnetic nanoparticles can be re-suspended due to the disappearance of the magnetic interaction. This feature eradicates the potential of agglomerate which may induce the thrombosis of blood vessels [40]. These magnetic properties indicate that DOX-loaded pH-MN is able to respond to an external magnetic field and shows high-trapping efficiency for magnetic targeting.

Additionally, the DLC and corresponding DLE were listed in Table 1. Both the DLC and DLE data demonstrate a descending trend with the decrease of Dex-COOH content. DOX was considered to be entrapped into the nanocarriers through electrostatic force. Dex-COOH provides negatively charged sites for the anchor of DOX. Less amount of Dex-COOH will result in low DLC and DLE value.

#### *pH-triggered dissociation and charge reversal*

The mild acid-triggered dissociation and charge reversal behavior of DOX-loaded pH-MN was monitored by



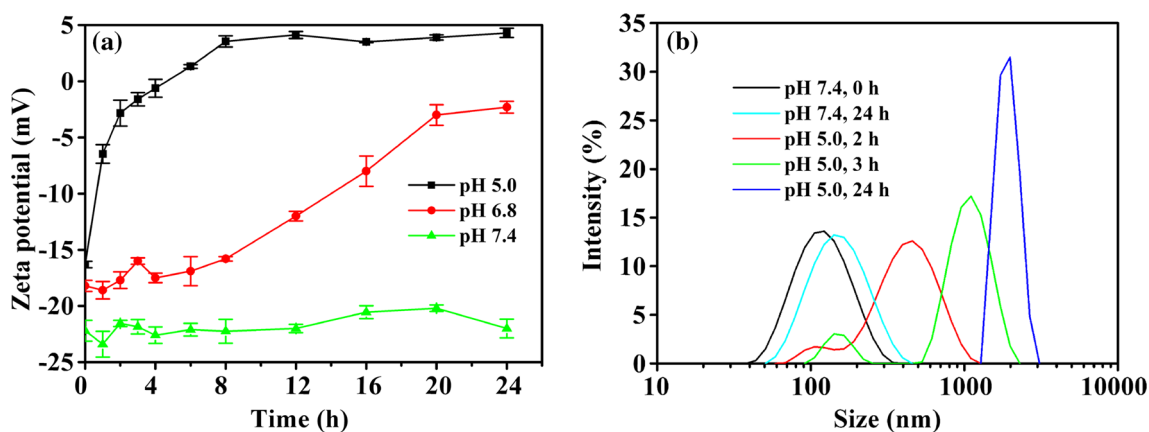


**Fig. 4** Zeta potential (a) and size (b) of DOX-loaded pH-MN2/1 in response to pH change for different periods of time, 0.1 mol/L PBS buffer at pH of 5.0, 6.8, and 7.4

tracking the size and zeta potential change of the particles under pH 5.0, 6.8, and 7.4 conditions at predetermined intervals by DLS, respectively.

The surface charge change was monitored for 24 h (Fig. 4a). No significant alteration was observed in the pH 7.4 environment. While in the pH 6.8 environment, the negative surface charge decreased and finally approached near to zero. However, the charge expressed instant and ostensible variation from negative to positive in pH 5.0 medium. These charge reversal behaviors are believed to be from the dissociation of citraconic amide linkage, which released positive amino group after the removal of negative carboxylic group [15, 16].

As is well known, the tumor extracellular pH (6.5–7.2), the endosome pH (5.0–6.5), and lysosome pH (4.5–5.0) are mildly acidic. The pH 6.8 medium was investigated herein for the sake of simulation of the tumor extracellular environment. Though it did not show positive at pH 6.8, the surface charge increased significantly. The similar alteration of surface charge values presumably occurs in the tumor extracellular environment. The variation benefits the endocytosis of nanocarriers. The reduction in negative charges will reduce the repulsion between nanocarriers and negatively charged cell membrane. This process may assist the uptake of nanocarrier and enhance their internalization by tumor cells. This observation is consistent with previous reports [15, 16, 41–43]. Moreover, when the nanocarriers were transferred to endosome/lysosome, the cleavage of amide linkage was strengthened and the surface charge of nanocarriers altered to positive, a case at pH 5.0. The repulsion forces between recovered amino groups and DOX may accelerate the disruption of the nanocarriers and trigger the release of DOX, which provide an intracellular enhanced drug delivery behavior. Therefore, the citraconic anhydride-modified structure is much better than the regularly occurring pH-sensitive linkage. The former will

incorporate extra feature of charge reversal other than the pH-sensitivity.

As shown in Fig. 4b, DOX-loaded pH-MN was very stable with single size distribution at pH 7.4. No significant size variation was monitored during the period of 24 h. However, when being exposed to pH 5.0, the size showed time-dependent variation (see Fig. 4b). For 2 h exposure to pH 5.0 medium, there appeared a reduced size peak, as expected. Other than that, there appeared another peak at increased size positions. As a matter of fact, the acidic medium brought about the disassembly of nanocarrier, however, the disassembled particles tended to aggregate because the loss of charges on the particles reduced the electrostatic repulsion among the particles and finally resulted in aggregation. As a consequence, increased size of particles was monitored. The samples would end up as precipitate. The observation after 24 h exposure to pH 5 medium, in fact, showed actual precipitation.

These experiments verified that the DOX-loaded pH-MN can be indeed disassembled under mildly acidic conditions and act as a drug carrier with the feature of pH-triggered release.

#### In vitro release study

To investigate the effect of pH on the drug release behavior, in vitro release experiments were conducted. The release profiles are plotted in Fig. 5. As shown in Fig. 5a, the nanocarrier exhibited a typical pH-responsive release. Three different pH conditions were explored upon the cumulative release percentage. It is obvious that pH 5.0 triggered significantly quicker and higher release than the pH 6.8 and pH 7.4 medium, respectively. pH 6.8 medium caused a lower release rate than pH 5.0 medium. As anticipated, pH 7.4 medium did reveal the lowest release among the three pH media. Specifically, an instant and

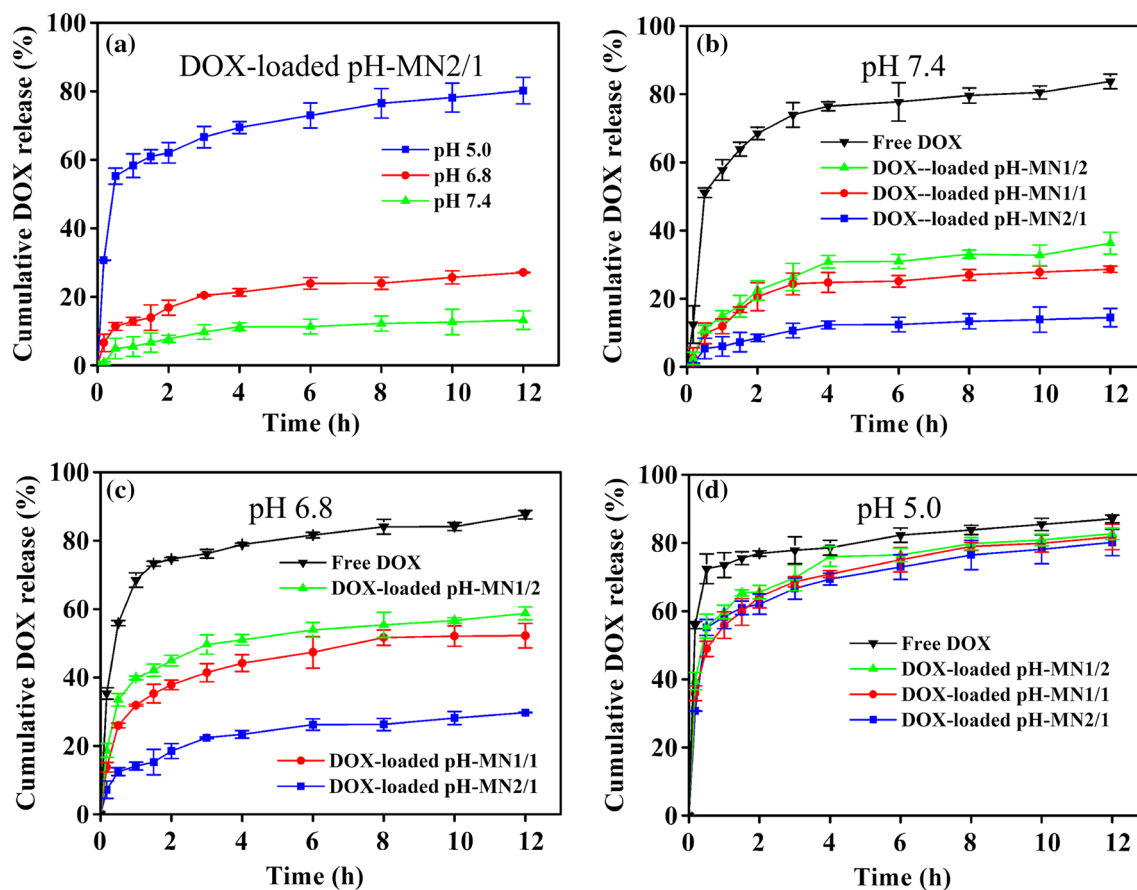


**Fig. 5** In vitro drug release of DOX-loaded pH-MN2/1 (a), DOX-loaded pH-MN at pH 7.4 (b), pH 6.8 (c), and pH 5.0 (d) using 0.1 mol/L PBS as the buffer solution

noticeable increase in release rate (the initial slope of the release curve) and in the cumulative release from pH 6.8 to 5.0 was monitored, while the corresponding increase from pH 7.4 to 6.8 was insignificant, as a sharp contrast. This elaborated that the carriers are typically pH-sensitive.

Nanocarriers prepared in different formulations displayed significant differences in release profile, shown in Fig. 5b–d. The purpose is for further illustration of the mechanisms of pH-controlled release. It is assumed that there are two mechanisms to trigger the release of DOX. One is related with electrostatic interaction whereas the other is the acid-induced cleavage of Dex–COOH. The modified dextran acts as the matrix which holds SPION and DOX. Apparently, the higher content of modified dextran would provide more anchors via electrostatic interaction to hold DOX, resulting in a slower release. In pH 7.4 medium (Fig. 5b), the pH-MN2/1 exhibited the lowest release ability, whereas the pH-MN1/2 revealed the highest release ability. These results are in full agreement with the analysis above. To note, the nanocarriers are very stable, or the electrostatic attraction is seldom destroyed in this case. When pH is lowered to 6.8,

the electrostatic interaction between DOX and Dex–COOH became weak. All the cumulative release increased in contrast with the corresponding cases in pH 7.4 medium (Fig. 5c). But still, the high content of Dex–COOH (pH-MN2/1) reveals a low release. When pH is further lowered to 5.0, citraconic amide linkage will be cleaved instantly. DOX will be released quickly and completely, regardless of the content of Dex–COOH in the nanocarrier. No significant difference in cumulative release was observed (Fig. 5d). Additionally, the total release amount nearly reached the level of the case of free DOX in dialysis tube. The observation elicited that the nanocarrier is typically pH-sensitive and the loaded DOX was entirely released. These studies support the feasibility that DOX-loaded pH-MN will release DOX efficiently at the endo-/lysosomal pH. Briefly, upon the comparison of release profiles in three different pHs, pH-MN2/1 displays the lowest release in pH 6.8 and pH 7.4. This kind of nanocarrier favors the reduced premature drug release during circulation but specifically enhances intracellular drug release, which will be definitely beneficial to effective cancer treatment.

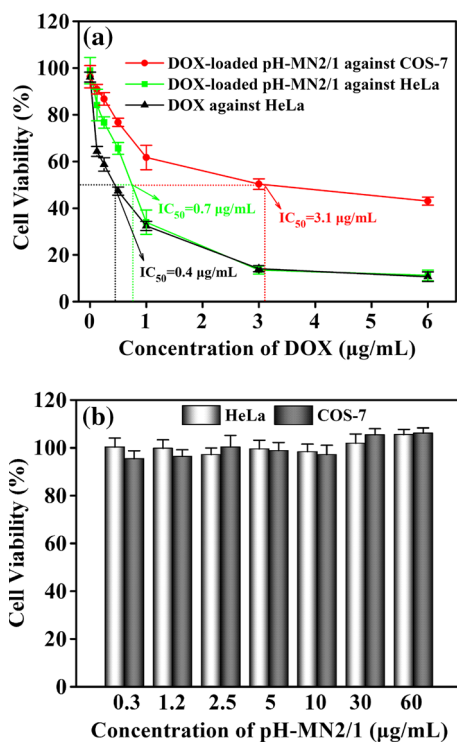


**Fig. 6** Cytotoxicity study of DOX-loaded pH-MN2/1 (a) and pH-MN2/1 (b) against HeLa cells and COS-7 cells after incubation for 48 h. The error bars represent standard deviation of eight independent experiments

To be noted, however, the magnetic migration will be weaker with the continuing increase of the dextran content. In this work, pH-MN2/1 was chosen as a candidate.

Cell study

Cytotoxicity assay

A MTT assay was performed to evaluate the viability of cells. As shown in Fig. 6a, the DOX-loaded pH-MN2/1 exhibited significant cytotoxicity with  $IC_{50}$   $0.7 \mu\text{g mL}^{-1}$

**Fig. 7** Microscopic images of Prussian blue-stained iron in HeLa cells: control of untreated cells (a) and pH-MN2/1-treated cells (b) for 24 h

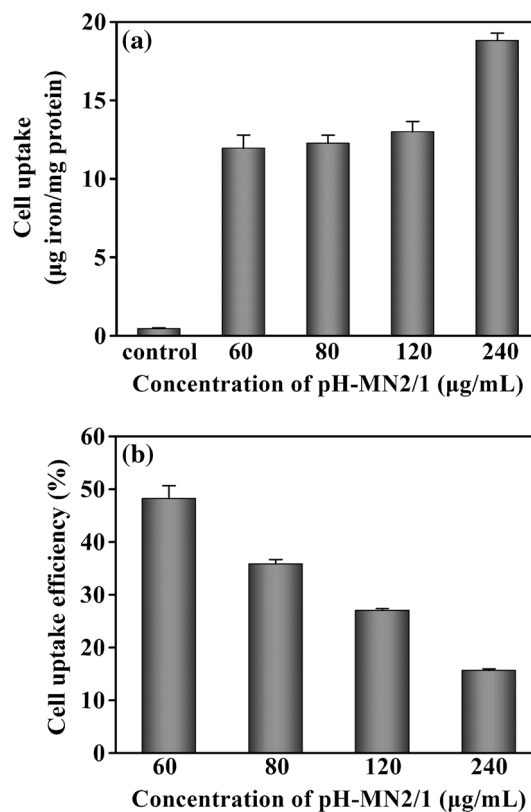
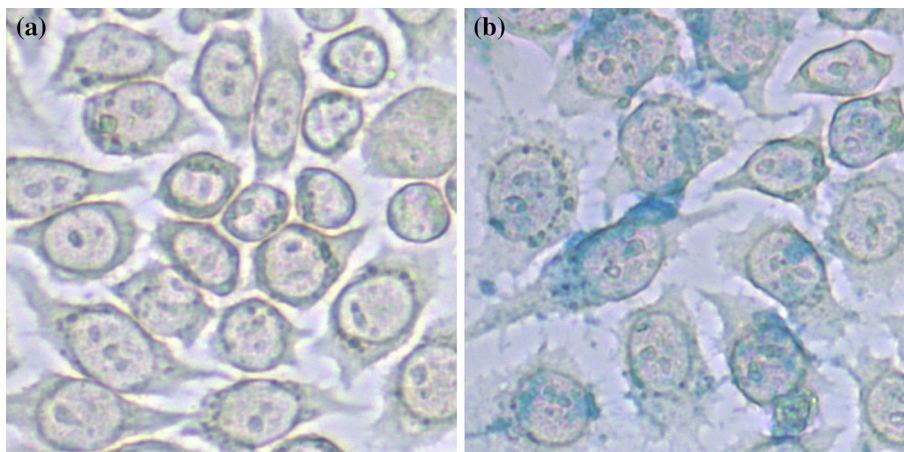


**Fig. 8** Quantification of iron concentration (a) and cellular uptake efficiencies (b) of iron in HeLa cells after incubation with different concentrations of pH-MN2/1 for 24 h, untreated cells were used as controls

for HeLa cells. As a control, free DOX was examined and found that the  $IC_{50}$  is  $0.4 \mu\text{g mL}^{-1}$ . Taking COS-7 as normal cells, the  $IC_{50}$  ( $3.1 \mu\text{g mL}^{-1}$ ) was much larger than that of HeLa cells. The explanation to the difference lies in the intracellular pH difference. This suggests that the nanocarrier exhibits low toxicity to normal cells and is a highly efficient potential drug carrier.

Further, the plain nanocarrier (without DOX) has no toxicity to both of HeLa and COS-7 cells (Fig. 6b). This testified that the whole process for the preparation of nanocarrier, including the modification of dextran, did not result in any toxicity.

#### Cellular uptake

The cellular uptake and intracellular distribution of iron and DOX were evaluated with HeLa cells. Prussian blue-staining experiments, which detect the presence of iron inside the cells, were conducted to confirm the accumulation of the pH-MN2/1 (no DOX loaded) and investigate its cellular uptake. After incubation with pH-MN2/1 for 24 h, HeLa cells were stained with potassium ferrocyanide and visualized with reverse microscopy. The microscopic images are shown in Fig. 7. Compared with the blank group of untreated cells, the number of blue granules in the cell significantly increased when the pH-MN2/1 was applied in the cell culture test. This means that the nanocarriers could be rapidly taken up by the HeLa cells.

The enhanced cellular uptake of pH-MN2/1 with a high concentration was further confirmed by the quantification of cellular iron concentration (Fig. 8). Cells which were not exposed to the pH-MN2/1 were collected and measured as a control. The intracellular iron content was expressed in terms

of the protein amount of cell, while the cellular uptake efficiency of iron was determined in light of the iron content in cells normalized by the fed iron in the pH-MN2/1. It was shown that the intracellular iron content increased with the increase of pH-MN2/1 amount (Fig. 8a). In contrast, the cellular uptake efficiency decreased as the increase of the fed amount of iron (Fig. 8b). The iron concentration in cells reached  $18.8 \mu\text{g mg}^{-1}$  protein after incubation with  $0.24 \text{ mg mL}^{-1}$  pH-MN2/1 for 24 h. These results indicated that the dose-dependent increase of intracellular iron content is likely attributed to HeLa cell endocytosis of pH-MN2/1, rather than the effect of gravity.

To further demonstrate whether DOX-loaded pH-MN can be more efficiently internalized by cancer cells, experiments on the intracellular drug release of DOX-loaded pH-MN were performed on HeLa cells after treatment for 4 or 24 h, and their cellular distribution was evaluated by confocal laser scanning microscopy (CLSM) analysis. As shown in Fig. 9, cells incubated with pH-sensitive DOX-loaded pH-MN2/1 showed strong DOX fluorescence in the cytoplasm and nuclei after 4 h, indicating fast internalization of nanocarriers and rapid release of DOX inside the cells. With further incubation for 24 h, the DOX fluorescence intensity inside the cells increased and the accumulation of DOX in the cell nuclei became more evident than after 4 h of incubation. Cells incubated with

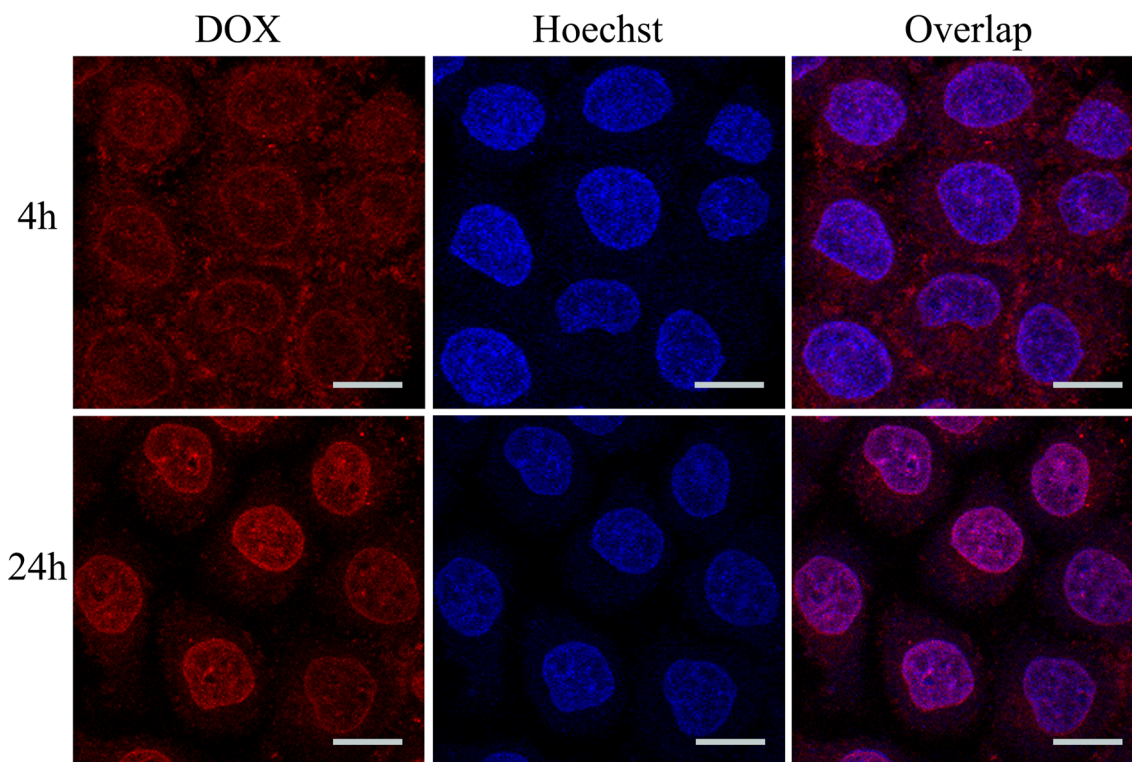


**Fig. 9** Confocal laser scanning microscopy images of HeLa cells after treatment with DOX-loaded pH-MN2/1 for 4 h (top) and 24 h (bottom). Red is DOX fluorescence, blue is cell nucleus treated with

hoechst 33258, and overlap. DOX dosage in the nanocarriers was  $0.7 \mu\text{g/mL}$ . Scale bar was  $20 \mu\text{m}$  (Color figure online)



DOX-loaded pH-MN presented strong DOX fluorescence in the cytoplasm and nuclei. The images indicated the rapid release of DOX from DOX-loaded pH-MN and its localization in nuclei. The observation can be attributed to the fast cleavage of citraconic amide in response to the intracellular acidic environment. Consequently, the burst release of DOX from the disrupted nanocarriers can be readily diffused into the nuclei. This result revealed that DOX-loaded pH-MN showed higher cytotoxicity because of the accumulation of DOX in its intracellular active site (nuclei), which enhanced its effect. Taken together, the DOX-loaded pH-MN exhibits significantly enhanced cellular internalization.

## Conclusion

In this study, a pH-responsive DOX-loaded magnetic nanoparticle as a drug nanocarrier has been demonstrated. The nanocarrier was able to efficiently deliver and release DOX into cancerous cells. The significant pH-responsiveness was introduced and readily regulated via citraconic anhydride-modified dextran in nanocarriers. SPION was assembled to provide the superparamagnetism, which imparts the nanocarrier the function of magnetic targeting and MRI. Charge reversal was achieved upon the treatment of mildly acidic medium. The resultant positive surface charge once favors the endocytosis and hence the cellular uptake of the nanocarrier. DOX was found to express the highest release rate at pH 5.0 environment, while the release was mostly inhibited at pH 7.4. Cellular uptake test and CLSM images indicated a fast internalization of the nanocarriers and efficient intracellular drug delivery, principally in nucleus. Therefore, DOX-loaded pH-MN are promising nanocarriers for a smart drug delivery system with magnetic targeting and pH-sensitivity, while providing the possibility of tracking using MRI technology.

**Acknowledgements** This research was supported by the National Natural Science Foundation of China (Grant No. 21071114), the Excellent Program of Activity of Science and Technology for Overseas-Returned Scientists founded by the Ministry of Human Resources and Social Security of the People's Republic of China, the Program for Innovative Research Teams of Hubei Provincial Department of Education, China, the project sponsored by the Scientific Research Foundation for Returned Overseas Chinese Scholars, State Education Ministry, the Key Natural Science Foundation of Hubei Province (2012FFA100), the Scientific Research Foundation of Wuhan Institute of Technology (10125032), and the Graduate Education Innovation Foundation of Wuhan Institute of Technology (CX2013014, CX2013032).

## References

1. Fleige E, Quadir MA, Haag R (2012) Stimuli-responsive polymeric nanocarriers for the controlled transport of active

- compounds: concepts and applications. *Adv Drug Deliv Rev* 64:866–884
2. Felber AE, Dufresne MH, Leroux JC (2012) pH-sensitive vesicles, polymeric micelles, and nanospheres prepared with polycarboxylates. *Adv Drug Deliv Rev* 64:979–992
  3. Du JZ, Du XJ, Mao CQ, Wang J (2011) Tailor-made dual pH-sensitive polymer–doxorubicin nanoparticles for efficient anti-cancer drug delivery. *J Am Chem Soc* 133:17560–17563
  4. Sankaranarayanan J, Mahmoud EA, Kim G, Morachis JM, Almutairi A (2010) Multiresponse strategies to modulate burst degradation and release from nanoparticles. *ACS Nano* 4:5930–5936
  5. Chen J, Qiu X, Ouyang J, Kong J, Zhong W, Xing MM (2011) pH and reduction dual-sensitive copolymeric micelles for intracellular doxorubicin delivery. *Biomacromolecules* 12:3601–3611
  6. Pennakalathil J, Jahja E, Özdemir ES, Konu Ö, Tuncel D (2014) Red emitting, cucurbituril-capped, pH-responsive conjugated oligomer-based nanoparticles for drug delivery and cellular imaging. *Biomacromolecules* 15:3366–3374
  7. Shi J, Liu Y, Wang L, Gao J, Zhang J, Yu X, Ma R, Liu R, Zhang Z (2014) A tumoral acidic pH-responsive drug delivery system based on a novel photosensitizer (fullerene) for in vitro and in vivo chemo-photodynamic therapy. *Acta Biomater* 10:1280–1291
  8. Meng F, Zhong Y, Cheng R, Deng C, Zhong Z (2014) pH-sensitive polymeric nanoparticles for tumor-targeting doxorubicin delivery: concept and recent advances. *Nanomedicine* 9:487–499
  9. Mailander V, Landfester K (2009) Interaction of nanoparticles with cells. *Biomacromolecules* 10:2379–2400
  10. Lee Y, Miyata K, Oba M, Ishii T, Fukushima S, Han M, Koyama H, Nishiyama N, Kataoka K (2008) Charge-conversion ternary polyplex with endosome disruption moiety: a technique for efficient and safe gene delivery. *Angew Chem* 120:5241–5244
  11. Cho EC, Xie J, Wurm PA, Xia Y (2009) Understanding the role of surface charges in cellular adsorption versus internalization by selectively removing gold nanoparticles on the cell surface with a I2/KI etchant. *Nano Lett* 9:1080–1084
  12. Huang Y, Tang Z, Zhang X, Yu H, Sun H, Pang X, Chen X (2013) pH-Triggered charge-reversal polypeptide nanoparticles for cisplatin delivery: preparation and in vitro evaluation. *Biomacromolecules* 14:2023–2032
  13. Xu P, Van Kirk EA, Zhan Y, Murdoch WJ, Radosz M, Shen Y (2007) Targeted charge-reversal nanoparticles for nuclear drug delivery. *Angew Chem Int Ed* 46:4999–5002
  14. Luo GF, Chen WH, Liu Y, Zhang J, Cheng SX, Zhuo RX, Zhang XZ (2013) Charge-reversal plug gate nanovalves on peptide-functionalized mesoporous silica nanoparticles for targeted drug delivery. *J Mater Chem B* 1:5723–5732
  15. Mok H, Park JW, Park TG (2008) Enhanced intracellular delivery of quantum dot and adenovirus nanoparticles triggered by acidic pH via surface charge reversal. *Bioconj Chem* 19:797–801
  16. Zhou T, Zhou X, Xing D (2014) Controlled release of doxorubicin from graphene oxide based charge-reversal nanocarrier. *Biomaterials* 35:4185–4194
  17. Veiseh O, Gunn JW, Zhang M (2010) Design and fabrication of magnetic nanoparticles for targeted drug delivery and imaging. *Adv Drug Deliv Rev* 62:284–304
  18. Min KA, Shin MC, Yu F, Yang M, David AE, Yang VC, Rosania GR (2013) Pulsed magnetic field improves the transport of iron oxide nanoparticles through cell barriers. *ACS Nano* 7:2161–2171
  19. Min KA, Yu F, Yang VC, Zhang X, Rosania GR (2010) Transcellular transport of heparin-coated magnetic iron oxide nanoparticles (Hep-MION) under the influence of an applied magnetic field. *Pharmaceutics* 2:119–135
  20. Domenech M, Marrero-Berrios I, Torres-Lugo M, Rinaldi C (2013) Lysosomal membrane permeabilization by targeted magnetic nanoparticles in alternating magnetic fields. *ACS Nano* 7:5091–5101

21. Nam J, Won N, Jin H, Chung H, Kim S (2009) pH-induced aggregation of gold nanoparticles for photothermal cancer therapy. *J Am Chem Soc* 131:13639–13645
22. Coué G, Freese C, Unger RE, James Kirkpatrick C, Engbersen JF (2013) Bioresponsive poly(amidoamine)s designed for intracellular protein delivery. *Acta Biomater* 9:6062–6074
23. Yu F, Huang Y, Cole AJ, Yang VC (2009) The artificial peroxidase activity of magnetic iron oxide nanoparticles and its application to glucose detection. *Biomaterials* 30:4716–4722
24. Hollander Z, Katchalski-Katzir E (1986) Use of monoclonal antibodies to detect conformational alterations in lactate dehydrogenase isoenzyme 5 on heat denaturation and on adsorption to polystyrene plates. *Mol Immunol* 23:927–933
25. Fields R (1971) The measurement of amino groups in proteins and peptides. *Biochem J* 124:581–590
26. Bataille I, Huguet J, Muller G, Mocanu G, Carpov A (1997) Associative behaviour of hydrophobically modified carboxymethylpullulan derivatives. *Int J Biol Macromol* 20:179–191
27. Liu WM, Xue YN, Peng N, He WT, Zhuo RX, Huang SW (2011) Dendrimer modified magnetic iron oxide nanoparticle/DNA/PEI ternary magnetoplexes: a novel strategy for magnetofection. *J Mater Chem* 21:13306–13315
28. Kim D, Zhang Y, Voit W, Rao K, Muhammed M (2001) Synthesis and characterization of surfactant-coated superparamagnetic monodispersed iron oxide nanoparticles. *J Magn Magn Mater* 225:30–36
29. Harris L, Goff J, Carmichael A, Riffle J, Harburn J, St. Pierre T, Saunders M (2003) Magnetite nanoparticle dispersions stabilized with triblock copolymers. *Chem Mater* 15:1367–1377
30. Yu F, Zhang L, Huang Y, Sun K, David AE, Yang VC (2010) The magnetophoretic mobility and superparamagnetism of core-shell iron oxide nanoparticles with dual targeting and imaging functionality. *Biomaterials* 31:5842–5848
31. Sun H, Guo B, Li X, Cheng R, Meng F, Liu H, Zhong Z (2010) Shell-sheddable micelles based on dextran-SS-poly( $\epsilon$ -caprolactone) diblock copolymer for efficient intracellular release of doxorubicin. *Biomacromolecules* 11:848–854
32. Liu X, Zhang J, Lynn DM (2008) Polyelectrolyte multilayers fabricated from 'charge-shifting' anionic polymers: a new approach to controlled film disruption and the release of cationic agents from surfaces. *Soft Matter* 4:1688–1695
33. Du YZ, Weng Q, Yuan H, Hu FQ (2010) Synthesis and antitumor activity of stearate-g-dextran micelles for intracellular doxorubicin delivery. *ACS Nano* 4:6894–6902
34. Culler S, Ishida H, Koenig J (1985) Structure of silane coupling agents adsorbed on silicon powder. *J Colloid Interf Sci* 106:334–346
35. Schmalenberg K, Frauchiger L, Nikkhouy-Albers L, Uhrich K (2001) Cytotoxicity of a unimolecular polymeric micelle and its degradation products. *Biomacromolecules* 2:851–855
36. Maeda H, Bharate G, Daruwalla J (2009) Polymeric drugs for efficient tumor-targeted drug delivery based on EPR-effect. *Eur J Pharm Biopharm* 71:409–419
37. Bautista MC, Bomati-Miguel O, del Puerto Morales M, Serna CJ, Veintemillas-Verdaguer S (2005) Surface characterisation of dextran-coated iron oxide nanoparticles prepared by laser pyrolysis and coprecipitation. *J Magn Magn Mater* 293:20–27
38. Durmus Z, Kavas H, Toprak MS, Baykal A, Altınçekiç TG, Aslan A, Bozkurt A, Coşgun S (2009) L-lysine coated iron oxide nanoparticles: synthesis, structural and conductivity characterization. *J Alloy Compd* 484:371–376
39. Kayal S, Ramanujan R (2010) Doxorubicin loaded PVA coated iron oxide nanoparticles for targeted drug delivery. *Mater Sci Eng C* 30:484–490
40. Guo L, Ding W, Zheng LM (2013) Synthesis and evaluation of c(RGDyK)-coupled superparamagnetic iron oxide nanoparticles for specific delivery of large amount of doxorubicin to tumor cell. *J Nanopart Res* 15:1–9
41. Gratton SE, Ropp PA, Pohlhaus PD, Luft JC, Madden VJ, Napier ME, DeSimone JM (2008) The effect of particle design on cellular internalization pathways. *Proc Natl Acad Sci USA* 105:11613–11618
42. Zhou Z, Shen Y, Tang J, Fan M, Van Kirk EA, Murdoch WJ, Radosz M (2009) Charge-reversal drug conjugate for targeted cancer cell nuclear drug delivery. *Adv Funct Mater* 19:3580–3589
43. Zhou Z, Shen Y, Tang J, Jin E, Ma X, Sun Q, Zhang B, Van Kirk EA, Murdoch WJ (2011) Linear polyethyleneimine-based charge-reversal nanoparticles for nuclear-targeted drug delivery. *J Mater Chem* 21:19114–19123